



HAL
open science

Mechanisms of Radical Formation on Chemically Modified Graphene Oxide under Near Infrared Irradiation

Lucas Jacquemin, Zheng Mei Song, Nolwenn Le Breton, Yuta Nishina, Sylvie Choua, Giacomo Reina, Alberto Bianco

► **To cite this version:**

Lucas Jacquemin, Zheng Mei Song, Nolwenn Le Breton, Yuta Nishina, Sylvie Choua, et al.. Mechanisms of Radical Formation on Chemically Modified Graphene Oxide under Near Infrared Irradiation. *Small*, 2023, 10.1002/sml.202207229 . hal-04020476

HAL Id: hal-04020476

<https://hal.science/hal-04020476>

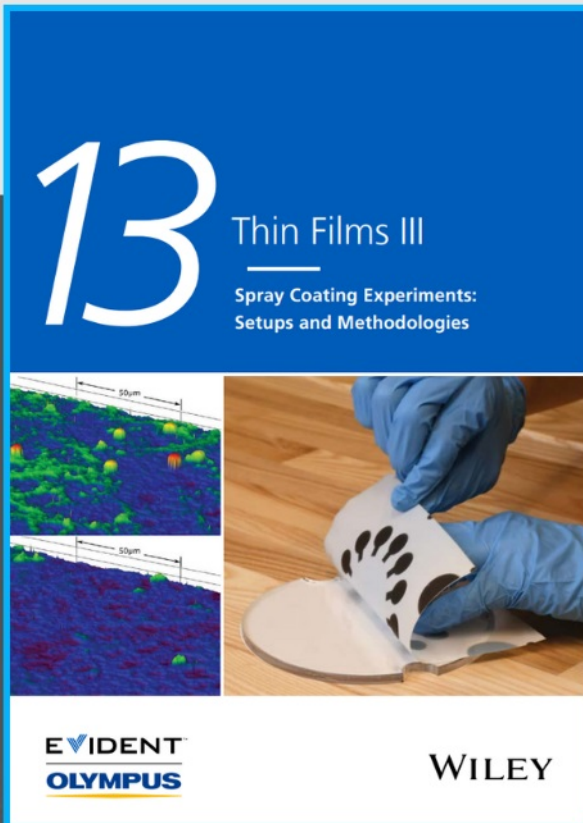
Submitted on 8 Mar 2023

HAL is a multi-disciplinary open access archive for the deposit and dissemination of scientific research documents, whether they are published or not. The documents may come from teaching and research institutions in France or abroad, or from public or private research centers.

L'archive ouverte pluridisciplinaire **HAL**, est destinée au dépôt et à la diffusion de documents scientifiques de niveau recherche, publiés ou non, émanant des établissements d'enseignement et de recherche français ou étrangers, des laboratoires publics ou privés.



Spray Coating Experiments: Setups and Methodologies



**The latest eBook from
Advanced Optical Metrology.
Download for free.**

Spray Coating Experiments: Setups and Methodologies, is the third in our Thin Films eBook series. This publication provides an introduction to spray coating, three article digests from Wiley Online Library and the latest news about Evident's Image of the Year Award 2022.

Wiley in collaboration with Evident, are committed to bridging the gap between fundamental research and industrial applications in the field of optical metrology. We strive to do this by collecting and organizing existing information, making it more accessible and useful for researchers and practitioners alike.

EVIDENT
OLYMPUS

WILEY

Mechanisms of Radical Formation on Chemically Modified Graphene Oxide under Near Infrared Irradiation

Lucas Jacquemin, Zhengmei Song, Nolwenn Le Breton, Yuta Nishina, Sylvie Choua, Giacomo Reina,* and Alberto Bianco*

In this work, the mechanisms of radical generation on different functionalized graphene oxide (GO) conjugates under near-infrared (NIR) light irradiation are investigated. The GO conjugates are designed to understand how chemical functionalization can influence the generation of radicals. Both pristine and functionalized GO are irradiated by a NIR laser, and the production of different reactive oxygen species (ROS) is investigated using fluorimetry and electron paramagnetic resonance to describe the type of radicals present on the surface of GO. The mechanism of ROS formation involves a charge transfer from the material to the oxygen present in the media, via the production of superoxide and singlet oxygen. Cytotoxicity and effects of ROS generation are then evaluated using breast cancer cells, evidencing a concentration dependent cell death associated to the heat and ROS. The study provides new hints to understand the photogeneration of radicals on the surface of GO upon near infrared irradiation, as well as, to assess the impact on these radicals in the context of a combined drug delivery system and phototherapeutic approach. These discoveries open the way for a better control of phototherapy-based treatments employing graphene-based materials.

1. Introduction

Carbon-based nanomaterials exist in different forms, and the key which links all these nanomaterials lies in the high percentage of carbon atoms connected through sp^2 or sp^3 bonds. The small size and the different properties of these materials stir a strong interest in different application fields from electronics to biomedicine. Especially, carbon-based nanomaterials have received a growing interest due to their interaction with light.^[1] This property can be exploited in a wide variety of applications, including phototherapy. The therapeutic benefit of phototherapy lies on an easy and flexible control of the light irradiation, the possibility to treat specific localized areas, as well as control time and dose of the therapeutic action.^[2] Depending on their interaction with light, two classes of phototherapies can operate. The first is the photothermal therapy


(PTT), which consists of the conversion of the adsorbed light by a material into surface vibrations producing heat. The local increase of the temperature can induce photoablation of tumor cells.^[3] The second is the photodynamic therapy (PDT), where the interaction with light produces free radicals and, most importantly, reactive oxygen species (ROS). This leads to high oxidative stress that destabilizes cell machinery and induces apoptosis.^[4] PDT is currently the most explored type of phototherapy for cancer treatment. Compared to PTT, PDT was already approved by FDA.^[5]

Within the different classes of carbon materials, graphene family nanomaterials have gained a lot of consensus as tools in cancer therapy. They are composed of hexagonal rings of carbon with electron delocalization depending on the type of graphene material.^[6] These 2D materials are good photothermal agents due to their ability to absorb at near-infrared (NIR) wavelengths.^[7]

Graphene generally shows poor colloidal stability, and this limits its use in drug delivery.^[8] Graphene oxide (GO) is the oxidized form of graphene. The oxidative synthesis process enriches GO surface with a wide variety of organic groups such as epoxides, hydroxyl and carboxyl groups.^[8] Because of its biocompatibility, hydrophilicity, high colloidal stability, and versatile surface chemistry, the biomedical applications of GO have been widely explored. In addition, GO can be easily

L. Jacquemin, Z. Song, G. Reina,^[†] A. Bianco
CNRS
Immunology
Immunopathology and Therapeutic Chemistry
UPR 3572
University of Strasbourg
ISIS
Strasbourg 67000, France
E-mail: giacomo.reina@empa.ch; a.bianco@ibmc-cnrs.unistra.fr
N. Le Breton, S. Choua
Institute of Chemistry
UMR 7177
University of Strasbourg
Strasbourg 67000, France

Y. Nishina
Graduate School of Natural Science and Technology
Okayama University
3-1-1 Tsushimanaka, Kita-ku, Okayama 700-8530, Japan

 The ORCID identification number(s) for the author(s) of this article can be found under <https://doi.org/10.1002/smll.202207229>.

© 2023 The Authors. Small published by Wiley-VCH GmbH. This is an open access article under the terms of the Creative Commons Attribution License, which permits use, distribution and reproduction in any medium, provided the original work is properly cited.

^[†]Present address: Empa Swiss Federal Laboratories for Materials Science and Technology Lerchenfeldstrasse 5, 9014 St. Gallen, Switzerland

DOI: 10.1002/smll.202207229

functionalized via covalent approaches with the help of oxygen functions present on its surface and through different non-covalent approaches (π - π stacking, H-bonding, etc.).^[8–10] These types of surface modifications allow to tune the nanomaterial properties and to unlock GO applications especially into the drug delivery field. Additionally, GO has been extensively used for PTT and or in a combined chemo/PTT treatment.^[11]

One of the main drawbacks on the use of GO in the biomedical field is its potential toxicity. GO toxicity depends on lateral size and surface chemistry.^[12] GO toxicity can be associated to the generation of ROS into the cell culture conditions.^[13] These free radicals are particularly toxic to cell membranes. The nature of the radicals presents onto the surface and at the edges of GO is complex and still under study.^[14–16] This source of reactivity relies on the defect contained onto GO surface that leads to the formation of localized unpaired electrons.^[17] The presence of these radicals allows GO to possess a high catalytic activity.^[18] For instance, GO can easily oxidize luminol in solution via radical reaction.^[14] In addition, recent studies demonstrated that graphene materials could catalyze benzylamine oxidation through oxygen activation (e.g., superoxide formation), and the yield of this reaction is temperature dependent.^[15] Besides, the “on demand” production of radical is highly desirable for PDT. For example, a study has shown that GO radical formation can be induced by heat and could be activated by NIR irradiation.^[15] Photogeneration of ROS under visible light was also studied to establish the potential hazards of GO to ecological systems.^[19] In contrast to NIR irradiation, the mechanism describing the reactivity of GO under UV irradiation is well described.^[20] Indeed, the combination of ultrafast time-resolved electron diffraction and time-resolved infrared vibrational spectroscopy allowed to identify how the energy applied via UV light can trigger a cascade of electron delocalization in the different energy bands of GO, leading to an energetic delocalization resulting in a charged or excited state induced oxygen loss. This mechanism can explain the generation of ROS.

Herein, the aim was to investigate whether the presence of the radicals on the surface of GO was affected by NIR irradiation, elucidate the mechanism and the type of radicals generated, and play with surface chemistry to enhance the ROS formation under NIR irradiation. For this purpose, we prepared different materials based on the covalent grafting of Diels–Alder product, obtained by the combination of furan and maleimide derivatives, onto small GO sheets. As a control, furfurylamine was employed as this molecule can be directly linked covalently with GO.^[21] The different derivatives were evaluated for their capacity to generate ROS under NIR irradiation, including superoxide ($O_2^{\cdot-}$), hydroxyl radicals (HO^{\cdot}), and singlet oxygen (1O_2). All these ROS display a high reactivity and can increase the therapeutic efficiency of the phototherapy. Then, the cytotoxicity of our materials, the photothermal and photodynamic effect induced against MCF-7 breast cancer cell line were evaluated. By combining the results of this study, we found that functionalization can modulate the ROS generation without a consistent change in the generation mechanism. Finally, we proved that functionalization improved the safety of the material, while maintaining its ability to kill the MCF-7 under NIR irradiation. These results are the first example of combined GO-based PDT and PTT for cancer therapy using NIR irradiation. We believe

that the knowledge on the NIR photogeneration of radicals onto the surface of GO is a crucial step to improve the efficiency of this type of materials in cancer therapy.

2. Results and Discussion

2.1. Design and Synthesis of Graphene Oxide Conjugates

In this work, we have synthesized different GO materials to obtain a multifunctional platform active for phototherapy under NIR irradiation and behaving as a drug delivery system. The key point of this work was to find appropriate functional groups able to induce a difference in radical generation upon covalent modification of GO surface. For this purpose, GO was functionalized with Diels–Alder (DA) derivatives as it has been already used in the construction of other drug delivery system.^[22] In the case of GO conjugates developed in this work, the DA reaction was performed between a furan ring (diene) and different maleimides (dienophiles). The choice of this type of DA was based on several points that we wanted to explore. First, we wanted to create a stable covalent bond between the DA molecule and the surface of GO to avoid undesired release, likely occurring when molecules are physisorbed on the sheets, whereas maintaining the opportunity to further functionalize the surface of GO covalently or non-covalently with other molecules. An efficient strategy, compatible with mild conditions, is to open the epoxide rings present onto the surface of GO by primary amine. Thereby, we performed the early preparation of DA molecules based on furfurylamine since the in situ preparation of the Diels–Alder process involves an increase of temperature while mild conditions are mandatory to maintain the hydration and the oxidation state of GO.^[10] Second, we wanted to use a functionalization able to stabilize and modulate the radical reactivity onto GO surface. Therefore, furfurylamine was chosen because it possesses a primary amine, and it is a good reductant,^[21] eventually able to tune radical formation. The introduction of a maleimide function then allowed us to modulate the reductive effect of our functionalization strategy. This modulation comes from the loss of electron delocalization on the furan ring via the switch from sp^2 to sp^3 hybridization. This allows to check if the reductive effect of the functionalization has an impact on ROS generation. In addition, the use of N-substituted maleimides allows to introduce groups with different electronegativity and hybridization. Therefore, we decided to use methyl and phenyl as substitutes for nitrogen. Indeed, the use of phenyl brings two different characteristics: a higher electronegativity compared to the methyl group and a possible stabilization of the free radicals through its π -conjugated system. The different Diels–Alder derivatives were synthesized following literature protocols (Figure S1, Supporting Information).^[23] N-substituted maleimides and furfurylamine were put at 90 °C overnight in toluene. At this temperature, only the exo isomers are formed. Indeed, we wanted to obtain the exo form to avoid the retro Diels–Alder reaction, occurring at a higher temperature than in the case of endo isomer, making the compound more thermally resistant for a PTT use.^[24] The products derived from this cycloaddition were isolated by column chromatography with a yield of $\approx 60\%$. The synthesized products

were characterized by mass spectrometry, HPLC, ^1H and ^{13}C NMR, and FT-IR (Figures S1–S6, Supporting Information). The resonances at 2–3 ppm in the ^1H NMR spectra corresponding to the protons linked to the diastereomeric carbons confirmed the presence of the exo isomers.^[24]

The starting GO was obtained by Hummers oxidation of graphite,^[25] leading to an aqueous dispersion at the concentration of 3 mg mL^{-1} . From SEM and TEM images, single layer GO sheets were observed, with an average size of $600 \pm 300\text{ nm}$ (Figure S9, Supporting Information). This size was selected because this GO can be easily taken up by cells,^[26] and have a longer time blood circulation.^[27]

Functionalized GO Diels–Alder conjugates were prepared following a method previously reported by our team based on “ultramixing” (Figure 1).^[28] This protocol can disperse the material via a high circumferential speed, avoiding the aggregation of the reagents, induced by charge destabilization. Indeed, the negative charge present onto GO surface can interact with the positive charges of the amino groups inducing GO aggregation.^[29] This phenomenon results in a decrease of the colloidal stability of GO in water and in cell culture media. The ultramixed solutions between synthesized DA derivatives, commercial furfurylamine, and GO were further stirred for 12 h and the resulting dispersions were purified by dialysis.

To establish the loading of the functions and to check the surface chemistry of GO, XPS analysis was performed on each conjugate (Figure 2). As expected, the introduction of the different functional groups caused a clear change in the XPS spectra. Compared to starting GO mainly composed by C and O atoms, the introduction of furfurylamine and DA derivatives increased the quantity of N atoms. Notably, from C/O ratio of the functionalized materials no reduction of GO was observed during the functionalization step. High resolution spectra of N1s were recorded for all materials and functionalization clearly induced the formation of two peaks at 399.6 and 401.6 eV corresponding to amines and positively charged amines, respectively. In addition, functionalization raised a new contribution in the deconvolution peak of C1s at 286.0 eV. Even if this contribution overlaps with C–OH bonds, the little increase can be attributed to the formation of C–N bonds onto the surface of GO.^[30] The amount of functional groups was estimated looking to the survey spectra, which give a quantification of N atoms. Starting GO exhibited a negligible content of N (<0.4%) and

the introduction of the different organic functions significantly increased this number (see table at the bottom of Figure 2). For the calculation, the molecular weight of each function, the number of N atoms in the molecule as well as the value obtained with the starting GO were considered. The loading of furfurylamine and DA products was estimated as follows: 1.5 wt% of functionalization for GOFurf, 0.6 wt% for GOME, and 1.3 wt% for GOPhe.

2.2. Photothermal Activity

GO is one of the most efficient photothermal agents in the NIR region.^[31] The photothermal activity was estimated irradiating at 808 nm GO dispersions and measuring the temperature increase. GO at this wavelength can convert laser energy into thermal energy.^[32] NIR irradiation is also convenient for biomedical applications as organs and tissues are transparent at this wavelength.^[33] Different concentrations of GO dispersions were irradiated for 15 min at 3.5 W cm^{-2} (Figure 3A) or 10 min at 2 W cm^{-2} (Figure 3B). GO photothermal response is associated to its carbon sp^2 framework, which was negligibly altered by our covalent functionalization (Figure 2). However, we decided to investigate the photothermal efficiency of GOFurf. Using a concentration of $100\text{ }\mu\text{g mL}^{-1}$, GOFurf underwent a photoactivation similar to GO (Figure S10, Supporting Information). Both set of data were compared to water control. The heating performance was evaluated by subtracting the temperature at time 0. As shown in Figure 3A,B, we could observe a concentration-dependent and irradiation-dependent trend of the PTT activity. The temperature is mainly increasing between 0 and 5 min of irradiation, subsequently reaching a plateau. Concerning the difference induced by the two power densities, the increase of temperature is almost proportionally doubled. The data obtained by the irradiation with 3.5 W cm^{-2} helped us to choose the right concentration, limiting PTT possible side effects. Indeed, at $10\text{ }\mu\text{g mL}^{-1}$ (not shown), the increase is too low if we want to lower the power density to be closer to in vivo conditions using GO.^[34]

On the basis of these data, we decided to use GO at $25\text{ }\mu\text{g mL}^{-1}$ at 2 W cm^{-2} for the continuation of the study. At this concentration, the recorded temperature increased up to $7\text{ }^\circ\text{C}$. However, the measure corresponds to the bulk

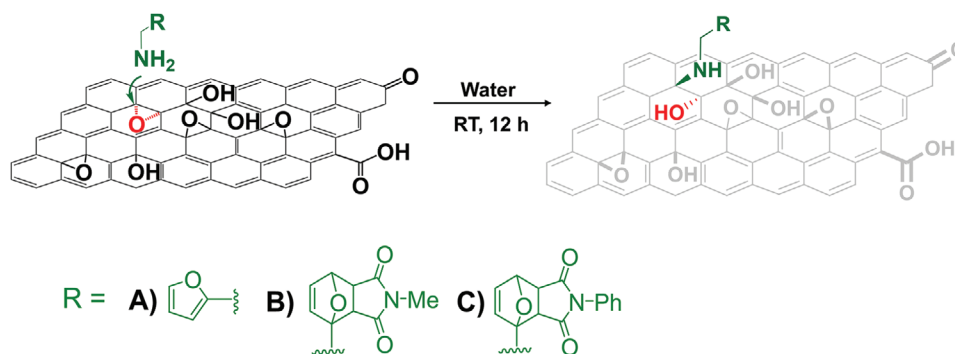
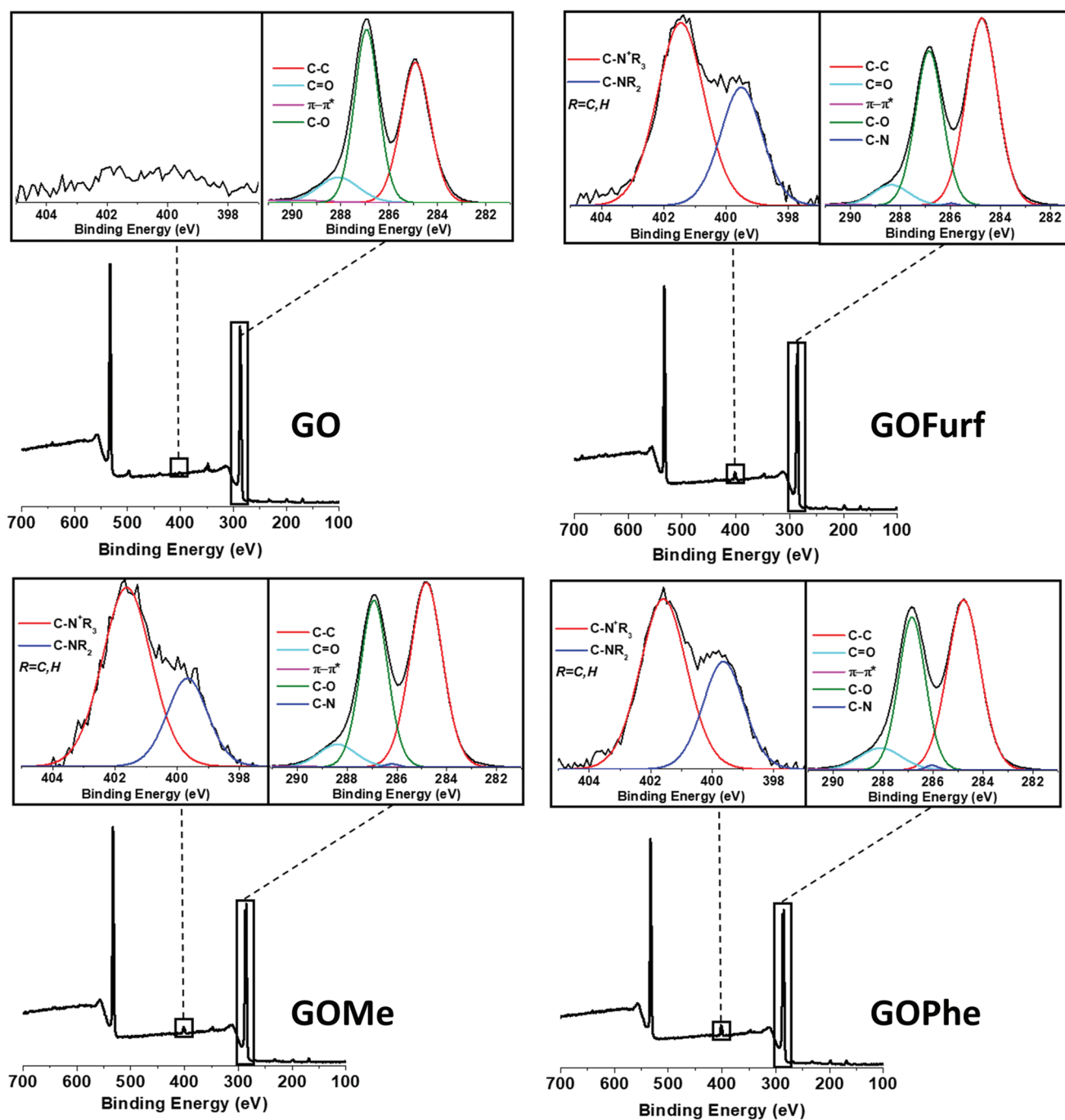


Figure 1. Functionalization of GO through epoxide ring opening with the different organic moieties. A) corresponds to furfurylamine, B) DANMe, and C) to DANPh. For the sake of clarity, only one epoxide is derivatized.



Element	GO [%]	GOFurf [%]	GOMe [%]	GOPhe [%]
C	68.0±0.2	71.8±0.6	71.4±0.2	71.5±0.8
O	31.6±0.2	26.3±0.6	26.9±0.1	25.5±1.2
N	0.4±0.1	1.9±0.1	1.6±0.3	3.0±0.5

Figure 2. XPS characterization. XPS survey spectra with high resolution N1s (left inset) and C1s (right inset) of GO (top left), GOFurf (top right), GOMe (middle left), and GOPhe (middle right). Bottom: Table reporting the relative XPS atomic percentage of C, O, and N. +decomposition of the DA products.

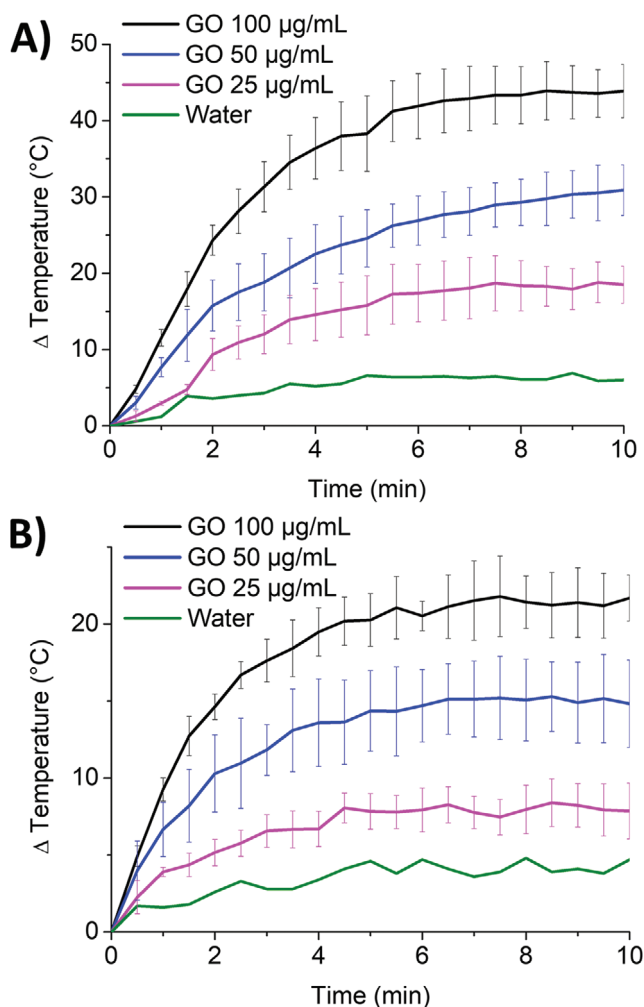


Figure 3. Photothermal response at 808 nm of GO at different concentrations. The temperature was recorded every 30 s. Data represent the mean value of 3 distinct experiments. Irradiation was performed with a power density of A) 3.5 W cm^{-2} , B) 2 W cm^{-2} .

temperature from the dispersion of the material. The accumulation of nanomaterials inside the cells can increase more the local temperature, leading to higher damages to the cells.^[35] During PTT, the stability of a molecule is essential. Under an increase of temperature, a possible retro Diels–Alder reaction can occur, leading to the decomposition of the DA products. Therefore, a control experiment was performed with the help of a fluorescent maleimide kit assay to quantify the retro Diels–Alder, which can occur for all functionalized materials during the irradiation time of 10 min using 2 W cm^{-2} . No maleimide formation was observed indicating that the synthesized ligands are stable during the irradiation conditions.

Therefore, a control experiment was performed with the help of a fluorescent maleimide kit assay to quantify the retro Diels–Alder, which can occur for all functionalized materials during the irradiation time of 10 min using 2 W cm^{-2} . No maleimide formation was observed indicating that the synthesized ligands are stable during the irradiation conditions.

2.3. Detection of Reactive Oxygen Species

GO is known to possess carbon radicals able to oxidize proteins, lipids, and other biological molecules.^[16,31] These radicals could be modulated by surface coating (e.g., protein coronation).^[16] As free radicals are known to generate ROS in the presence of oxygen or water molecules.^[37] In a previous work using HeLa cells, we found that GO displayed very low cytotoxic effects at this concentration.^[33] Moreover, other studies have shown that GO did not affect cell viability at $25 \mu\text{g mL}^{-1}$ in other types of cell lines. The methodology used to determine the ROS in aqueous solution and under NIR irradiation was based on the combination of fluorescent probes and EPR spin traps,^[34] allowing to understand the mechanism of formation and the type of radicals produced (Figure S2, Supporting Information). Each probe is sensitive to different types of ROS. Direct visualization of the radicals has been already shown by Vranick et al. measuring the EPR signals on freeze-dried GO.^[16] However, in our case direct radical measurement onto GO surface was not possible, most probably because of the low concentration of GO in solution.

Initially, we tested non-fluorescent probe dihydrorhodamine 123 (DHR123) as it is sensitive to a wide variety of ROS (e.g., HO^\bullet , $^1\text{O}_2$, and $\text{O}_2^{\bullet-}$) and to direct oxidation.^[35] The probe response is based on the conversion of DHR123 into fluorescent rhodamine 123 (Figure S2A, Supporting Information) with a maximum emission intensity at 526 nm following an excitation at 490 nm.

In particular, we reported the fluorescence normalized to DHR123. The control experiment of irradiated DHR123 did not show any increase of fluorescent signal. This is associated to the mild irradiation condition used and to the low ionizing capacity of NIR light. Immediately after incubating DHR123 with GO at $25 \mu\text{g mL}^{-1}$ in the dark, an increase of fluorescence was recorded (4-folds) (Figure 4a). The radical oxidation of the probe can be ascribed to the direct interaction of DHR123 with the unpaired spin present onto the GO surface or to the formation of an intermediate oxygenated species.^[14–16] Continuous incubation for 10 min in the same conditions did not show significant enhancement of the probe photoluminescence (6.5-folds). The latter is in accordance with the fast kinetic of radical reactions. When GO was instead irradiated at 808 nm for 10 min, an increase of 25 times was observed, associated to the production of photogenerated ROS. From this first set of experiment, we confirmed that GO was able to generate ROS in solution. This finding opens up the possibility to exploit such radicals generated by NIR irradiation for PDT. Similar to pristine GO, functionalized nanomaterials showed the same trend in the photooxidation capacity of DHR123. This behavior suggests that the functionalization with DA adducts of GO did not modify the radical reactivity of the conjugates toward DHR123. Unfortunately, DHR123 is not a NIR selective probe as it can be oxidized by different types of ROS.^[36] Following the proof that irradiation of functionalized or non-functionalized GO generate ROS, we decided to shed light on the photogenerated radical mechanism. For this reason, we used additional experiments that allowed the distinction of the type of the produced radical species. We combined the use of fluorescent probes and EPR spin trapping strategy. The latter method is based

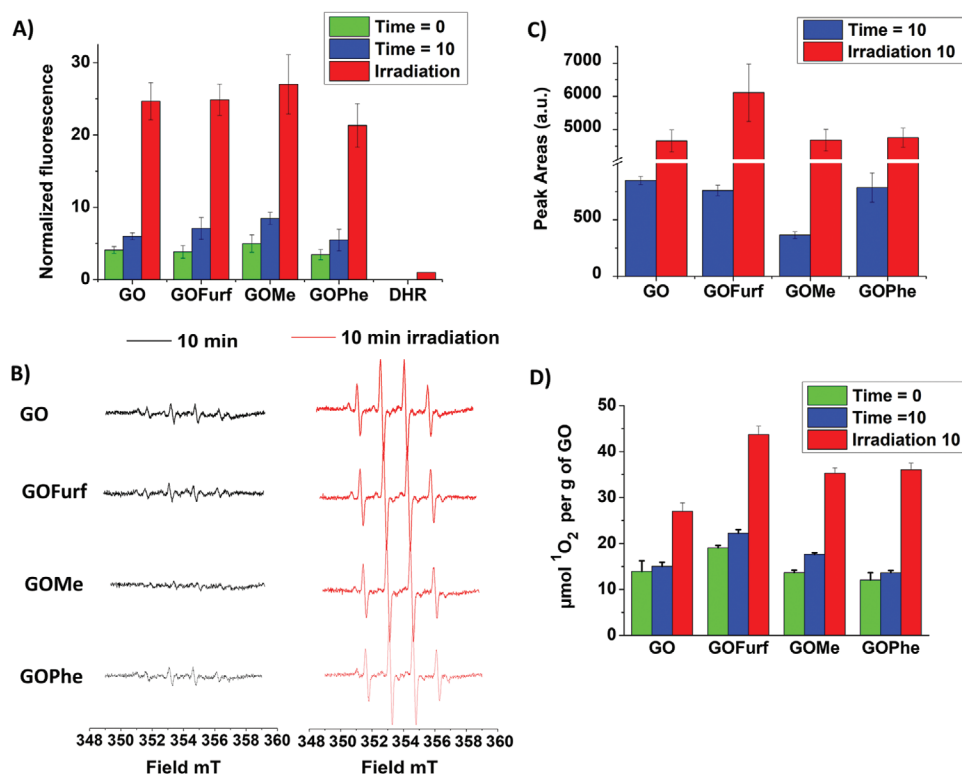


Figure 4. ROS detection. A) ROS levels ($\lambda_{\text{ex}} = 490$ nm, $\lambda_{\text{em}} = 526$ nm) after mixing DHR123 with GO materials for 0 or 10 min in the dark or under NIR for 10 min at 808 nm (2 W cm^{-2}). Data are normalized to the values obtained with DHR123 irradiated alone for 10 min under NIR at 808 nm. B) ROS levels from EPR spectra recorded by mixing GO materials with DMPO for 10 min in the dark or under NIR for 10 min at 808 nm. Signals are an average of 9 scans. C) Spectra ROS levels obtained integrating the area under the peak from right spectra in panel B. D) ROS levels ($\lambda_{\text{ex}} = 404$ nm, $\lambda_{\text{em}} = 490$ nm) after mixing ABDA with GO materials for 0 or 10 min in the dark or under NIR for 10 min at 808 nm (2 W cm^{-2}). Values were calculated from the data obtained with a calibration curve of ABDA concentration.

on the reaction between a radical, whose lifetime is too short to be detected under experimental conditions, and a diamagnetic reagent (spin trap) to form a stable spin adduct. The EPR spectra of the spin adducts are characteristic of the radical trapped^[34] (i.e., carbon species, oxygen species, etc.). It is thus easy to determine if the source of these radicals comes from the carbon radicals present on the surface of the GO or from an oxygen mediated mechanism.

First, we decided to use 5,5-dimethyl-1-pyrroline N-oxide (DMPO) as EPR probe. In Figure 4B, a signal of 4 lines with an intensity ratio of 1:2:2:1 corresponding to DMPO-OH was registered after 20 min in solution in the presence of GO.^[34] This time takes into account the initial 10 min in solution, similar to the condition with DHR123 probe, and 10 additional min necessary for spectrum accumulation in the EPR spectrometer. Text books state that stable radical species identified appear after reaction of molecules with hydroxyl radicals or superoxide or by their direct oxidation and leading to products containing an unpaired electron observable by EPR.^[34] Unfortunately, the intermediate forms (Figure S2, Supporting Information) after interaction between superoxide and DMPO or by direct oxidation, possesses an half-time too short (60 s at pH 7)^[37] to be observed under our conditions (10 min irradiation coupled with almost 10 min of spectral accumulation). Thus, only the final DMPOH-OH was observable (Figure S2B, Supporting Information). As previously observed with DHR123, irradiation

for 10 min in similar conditions increased the signal intensity with a similar factor (around 5–6-folds between non irradiated and irradiated samples). This result confirms by two different techniques the ability of GO to act as a photosensitizer when irradiated in the NIR region. However, comparing the oxidation of DMPO to DHR123, we can see a significant impact due to the functionalization either under irradiation or without irradiation. In the not irradiated experimental setting, it is clearly observable that GOMe produced an amount of radicals about 60% lower than pristine GO. Instead after irradiation, GOFurf conjugate showed a greater capacity of radical generation compared to GO (>30%). As we could still not identify the mechanism under the formation of DMPO-OH radical, we wanted to push this analysis further. In order to explain if DMPO-OH species were obtained by a direct oxidation or due to oxygen radicals, the experiments with DMPO were performed under deoxygenated atmosphere (Figure 5).

In this condition, no signals were observed even under NIR irradiation, meaning that molecular oxygen is involved in the radical photogeneration. Moreover, this can exclude a direct oxidation of DMPO. Following these results, a specific trap for hydroxyl radicals was selected, corresponding to α -(4-pyridyl N-oxide)-N-tert-butyl nitron (POBN) in ethanol (Figure S2C, Supporting Information). In this assay, ethanol was used as a trap for hydroxyl radicals, leading to generation of alkyl radicals reacting with POBN, with a characteristic profile in EPR

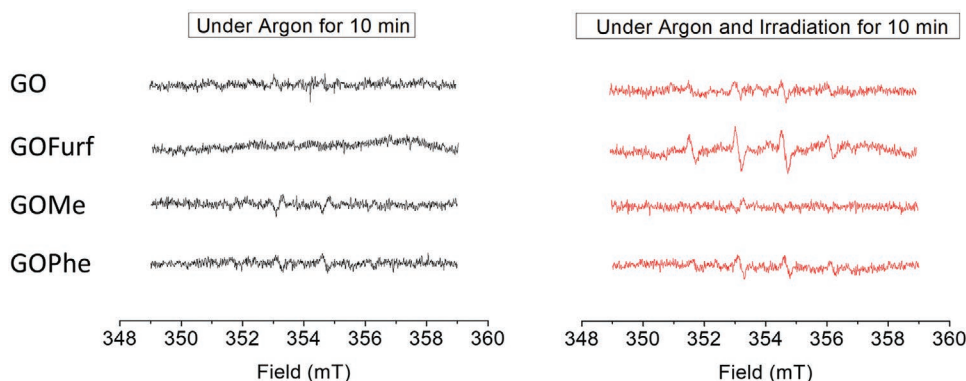


Figure 5. EPR spectra of GO conjugates mixed with DMPO under argon atmosphere for 10 min and for 10 min under NIR at 808 nm. Signals are average of 9 scans.

spectra.^[34] The four different conjugates gave no signals, even under NIR irradiation (Figure S11, Supporting Information). Therefore, we demonstrated that GO and functionalized GO did not generate hydroxyl radicals under photoirradiation. These results confirm the previous results obtained with DMPO which showed that oxygen was mandatory, supporting mainly the formation of superoxide and singlet oxygen.

9,10-Anthracenediyl-bis(methylene)dimalonic acid (ABDA) was used as a specific fluorescent probe to quantify singlet oxygen production. The reaction is specific for the detection of $^1\text{O}_2$ that reacts with the probe through a Diels–Alder addition of the singlet oxygen onto the anthracene ring (Figure S2D, Supporting Information), while other ROS species are not able to react with this probe. As the endoperoxide species (ABDA- O_2) is not fluorescent, $^1\text{O}_2$ production was monitored by following the loss of fluorescence emission intensity at 404 nm.^[35] As stated before, ABDA oxidation is selective to singlet oxygen, allowing the quantification of $^1\text{O}_2$ during the irradiation. For sake of comparison, we have expressed the concentration of $^1\text{O}_2$ per gram of GO during the irradiation process (Figure 4C). As observed with DHR123, a significant quantity of radicals was found when the probe was mixed with GO materials, whereas a slight decrease of fluorescence was observed after 10 min. In both cases, GOFurf seemed to generate more radicals, while for the other functions the difference is lower in comparison to GO. It is however already possible to establish a classification between the functions. Without irradiation the classification of ROS production is as follows: GOFurf (+45%) > GOMe (+15%) > GOPhe (–10%) compared to GO after 10 min. Under NIR irradiation for 10 min, the trend remains similar to that observed with the other probes; all materials exhibit more or less the double of radical production compared to the controls. Classification is again possible after NIR treatment, following: GOFurf ($\approx 60\%$) > GOMe ($\approx 30\%$) = GOPhe ($\approx 30\%$) compared to GO. In order to demonstrate that the oxidation was not due to a different mechanism than the singlet oxygen production evidenced in the experiment using ABDA, a final control was performed by EPR. For this purpose, 2,2,6,6-tetramethyl-4-piperidinol (TMP-OH), a specific spin trap for $^1\text{O}_2$, was used (Figure S12, Supporting Information). TMP-OH in contact with $^1\text{O}_2$ reacts to form TEMPOL, a paramagnetic molecule observable by EPR. As in the case of ABDA, a small but still significant amount of

radicals was observed without stimuli. Following the NIR irradiation, an increase in intensity of the signals of about 7 times was observed.

By combining the data obtained from the different probes, we found that the functionalization and the irradiation do not modify the nature of the photoproducted radicals, but rather their quantity. DMPO and DHR123 are not specific enough to evidence the exact type of radicals in our experimental conditions. However, spin trapping experiments using DMPO showed the formation of an oxygen based radical whose formation mechanism cannot support a direct oxidation. Additionally, all the materials are not able to oxidize POBN in ethanol excluding the production of hydroxyl radicals, hydrogen peroxide (detectable by POBN) and H_2O^{++} (precursor of HO^\bullet radicals). Furthermore, as ABDA is specific to singlet oxygen,^[38] and DHR123 and DMPO are sensitive to superoxide,^[39] we can assume the production of $^1\text{O}_2$ and $\text{O}_2^{\bullet-}$ during the irradiation process.

To establish a plausible mechanism for the generation of the radicals, it is necessary to look at both the data we have obtained and the literature. For molecular photosensitizers, the oxidation ratio between ABDA and DHR123 has been associated to the conversion ratio between triplet and single state generation ($^1\text{O}_2$) and charge transfer ($\text{O}_2^{\bullet-}$) during the photogeneration process.^[40] We found that superoxide and singlet oxygen are generated without stimuli and that their formation can be sensibly enhanced during NIR irradiation. Superoxide can be formed by radical oxidation of GO by O_2 . Subsequently, $\text{O}_2^{\bullet-}$ can remain adsorbed onto GO^{++} due to ionic interactions (Figure 6).^[15] GO was already shown to produce superoxide through NIR irradiation.^[41] It was also proved that the generation of superoxide occurs upon an increase of temperature.^[15] GO was able to oxidize luminol and be reactivated through a treatment with H_2O_2 , while a thermal treatment reduces the amount of carbon radicals.^[14]

These observations are in accordance with our experiments where we evidenced the oxidation of DHR123 and DMPO via $\text{O}_2^{\bullet-}$ formation. The most interesting finding of this study is the observation of singlet oxygen production. Indeed, singlet oxygen formation is usually mediated by an energy transfer from the excited triplet state of a photosensitizer to singlet oxygen.^[42] But, GO materials are able to produce this type of radicals even without stimuli (Figure 4 and Figure S10,

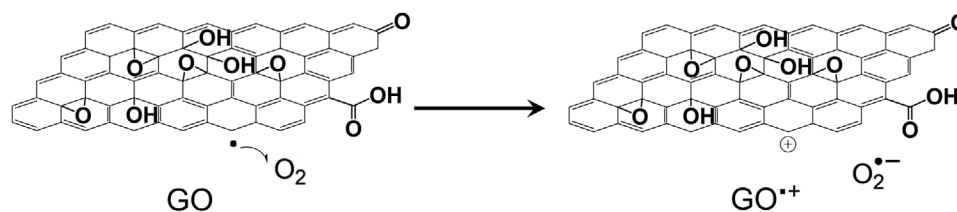


Figure 6. Radical oxidation of GO to form $O_2^{\bullet -}$.

Supporting Information). Besides, another mechanism has been proposed to produce singlet oxygen for non-triplet generating PDT sensitizer such as TiO_2 .^[42] In this case, singlet oxidation could be produced by oxidation of superoxide. This electron removal in the oxidation process can occur in three different ways due to three equivalents π -antibonding orbitals on superoxide. These three ways generate three energy excited states of O_2 : $^3\Sigma_g^-$, $^1\Delta_g$, and $^1\Sigma_g^+$. $^1\Sigma_g^+$ is energetically too high and converts into $^1\Delta_g$. Thus, the oxidation of superoxide generates with a probability of 2/5 singlet oxygen and 3/5 triplet oxygen.^[42] For the oxidative mechanism, two different ways to generate singlet were already described by the following equations:



In Equation (1), the reaction occurs due to a favorable energy involving the presence of HO^{\bullet} . The Equation (2) foresees the oxidation of superoxide due to a hole (carbocation radical) produced after the oxidation. In our experiments with POBN, the hydroxyl radical concentration was below the detection limits, making mechanism (1) unfavorable. On the other hand, reaction (2) involves oxidation performed by a cationic state of the material $GO^{\bullet +}$ (h). (Figure 6). When $GO^{\bullet +}$ is irradiated there is a high local temperature enhancement that induces an increase of reactivity. The oxidation/reduction of O_2 can be mediated by the different groups grafted onto GO surface. In particular, functionalized materials are able to reduce the $O_2^{\bullet -}$ (from DMPO oxidation), while similar amounts of 1O_2 were recorded (from ABDA oxidation) in non-irradiated condition. Viewing the potential toxicity of GO associated to the ROS formation, we have found that choosing the appropriate functionalization it is possible to alleviate ROS formation. Additionally, from our study we showed that during NIR irradiation GO works as a powerful photosensitizer, where the generation of 1O_2 can be maximized by surface functionalization of the material.

2.4. In Vitro Cell Viability Study

Because of their great tunability and versatility, phototherapies have emerged as new modalities for combined cancer therapy. They can overcome a lot of side effects on healthy tissues increasing the efficacy in killing primarily cancer cells.^[43] In this therapeutic context, it is imperative to evaluate the safety of our compounds without stimulus to ensure control over

cytotoxicity, in particular, because we detected radicals in our study without irradiation or stimulus in non-physiological environment. Therefore, GO materials were investigated against human breast cancer cell line MCF-7 by Live/Dead assay. For this purpose, the MCF-7 cells were incubated with the GO, GOFurf, GOME and GOPhe at different concentrations (10, 25, 50, 75, 100 $\mu\text{g mL}^{-1}$) for 24 h (Figure S13, Supporting Information). GO shows a time and a concentration dependent internalization, and 24 h of incubation is a sufficient incubation time for the material uptake.^[16,28,44] Then, the cells were washed, and the live/dead staining solution was added to test cell viability (Figure 7A). The functionalized GO materials (GOFurf, GOME, and GOPhe) altered very little, although statistically significantly, cell viability up to a concentration of 50 $\mu\text{g mL}^{-1}$ being cell survival being more than 90%. Pristine GO showed more toxicity than functionalized materials. At 100 $\mu\text{g mL}^{-1}$, the viability of cells treated with GO significantly decreased to 66%, while in the case of GOFurf, GOME, and GOPhe, the percentage of live cells was 80%, 75%, and 84%, respectively. We could observe that the GOME has a better dispersibility in the cell culture media than GO, that may be one of the reasons of its higher cytocompatibility compared to GO and the other functionalized GO.^[45,46] The functionalized GO displayed lower impact on cell viability, and this can be associated also to their lower ROS generation in solution.

2.5. In Vitro Combined Photothermal Therapy/Photodynamic Therapy

For evaluation of the combined PTT/PDT effect of GO and GO conjugates, the cell viability on MCF-7 was compared with and without irradiation using again live/dead assay. The aim of this experiment is to demonstrate the increase in toxicity of our compounds when irradiated at 808 nm (2 W cm^{-2}) associated to thermal increase (Figure 3) and ROS photogeneration (Figure 4). Since the two types of activation occur at the same wavelength, it was not possible to dissociate the contribution of PDT from that of PTT. As the three GO conjugates (GOFurf, GOME, and GOPhe) displayed similar cell viability effects (Figure 7A), GOME was chosen as the representative to test the phototherapy efficiency. The cells were treated with GO and GOME at 25 $\mu\text{g mL}^{-1}$, the same concentration used to assess the radical formation, for 24 h and then irradiated with NIR laser ($2 \text{ W} \cdot \text{cm}^{-2}$) at 808 nm for 10 min, followed by viability measurements after 24 h. As shown in Figure 4B, the cell viability was significantly decreased in response to NIR irradiation. Dead cells were 54% and 47% for GO and GOME, respectively, after the 10 min irradiation, in comparison to 16%

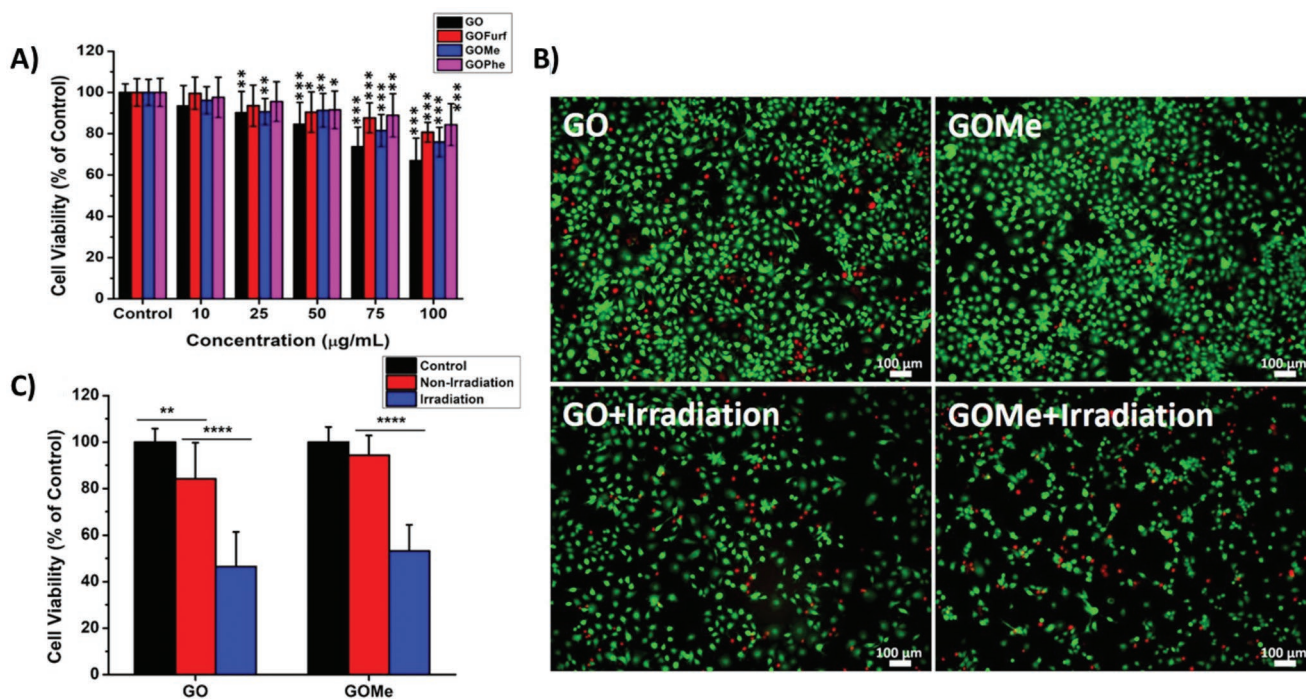


Figure 7. A) Cell viability of GO, GOFurf, GOMe, GOPhe at different concentrations on MCF-7 cells after exposed 24 h. B) Cell viability of MCF-7 cells after the treatment of $25 \mu\text{g mL}^{-1}$ GO or GOMe with or without laser irradiation (2 W cm^{-2}) at 808 nm for 10 min. C) Live/Dead images after laser irradiation (2 W cm^{-2}) at 808 nm for 10 min. Calcein-AM (Green, live cells), ethidium homodimer-1 (Red, dead cells). Magnification 5 \times . The results are expressed as the means \pm SD ($n \geq 3$). The statistical analyses were performed by the one-way ANOVA. $*p < 0.05$; $**p < 0.01$; $***p < 0.001$; $****p < 0.0001$ compared to the untreated control.

and 6% for non-irradiated groups, respectively. These results highlight again the positive effect of functionalization of GO in its use in PDT and PTT. Indeed, compared to GO, the simple surface modification with DA adducts sensibly reduces the basal ROS generated from the material, so alleviating its cytotoxicity while the functionalization does not hamper the high GO photocytotoxicity.

To further assess the combined photothermal and PDT effects of GO and GOMe, the live/dead images were recorded using calcein-AM and ethidium homodimer-1 fluorescence dyes to identify living (green) and dead (red) cells (Figure 7C). In addition, more cells were stained in red after irradiation. The cell morphology was also observed after laser irradiation, and their shape clearly changed, with many cells dead (Figure S14, Supporting Information). Overall, the irradiation effect not only inhibited the cell proliferation, but also induced cell death, revealing the key role of photothermal and PDT effects.^[47]

2.6. Intracellular Detection of Reactive Oxygen Species

We showed the good efficacy of the PDT/PTT of our materials. However, since a single NIR wavelength is used during irradiation, it is hard to study if this therapeutic outcome is mainly due to the ROS formation or to the local hyperthermia. While the photothermal effect depends mainly on the GO sp^2 structure, and is expected to not be changed by the functionalization, we have demonstrated that the ROS generation can be modulated by the surface modification of the material. All our

previous studies have been conducted in water, while the biological environment is much more complex where proteins or glutathione may prevent the ROS photogeneration of the material, comprising its PDT activity. For these reasons, we decided to assess the generation of ROS of GO and GOMe in MCF-7 cells. To capture the ROS in these cells, 2',7'-dichlorodihydrofluorescein diacetate (CM-H₂DCFDA) reagent was chosen as a probe. This dye is initially non-fluorescent in a reduced state and becomes fluorescent (green emission) upon oxidation by ROS.^[48] The MCF-7 cells were incubated with GO or GOMe (at $25 \mu\text{g mL}^{-1}$) for 24 h. After washing to remove the materials outside the cells, CM-H₂DCFDA reagent was added to monitor the intracellular ROS.

We observed that the ROS level of the MCF-7 cells was almost the same when exposed to GO or GOMe without irradiation. This is consistent with the cell viability where GO and GOMe show similar cytotoxicity at $25 \mu\text{g mL}^{-1}$ (Figure 8). On the other hand, we detected a significant CM-H₂DCFDA oxidation in both GO and GOMe after 10 min irradiation at 808 nm (2 W cm^{-2}) (Figure 8). Compared with GO under irradiation, GOMe is able to induce a higher radical stress in MCF-7 cells, although, this is not correlated to an obvious trend with the phototherapeutic efficacy (Figure 4). This may be due to different reasons, including different cell uptake and trafficking into cell. On the other hand, we have decided to use a low concentration of material to investigate on the possibility of using GO and functionalized GO for combined PDT and PTT. These results provide evidence that GOMe is able to produce an increase of oxidative stress, and consequently a higher level

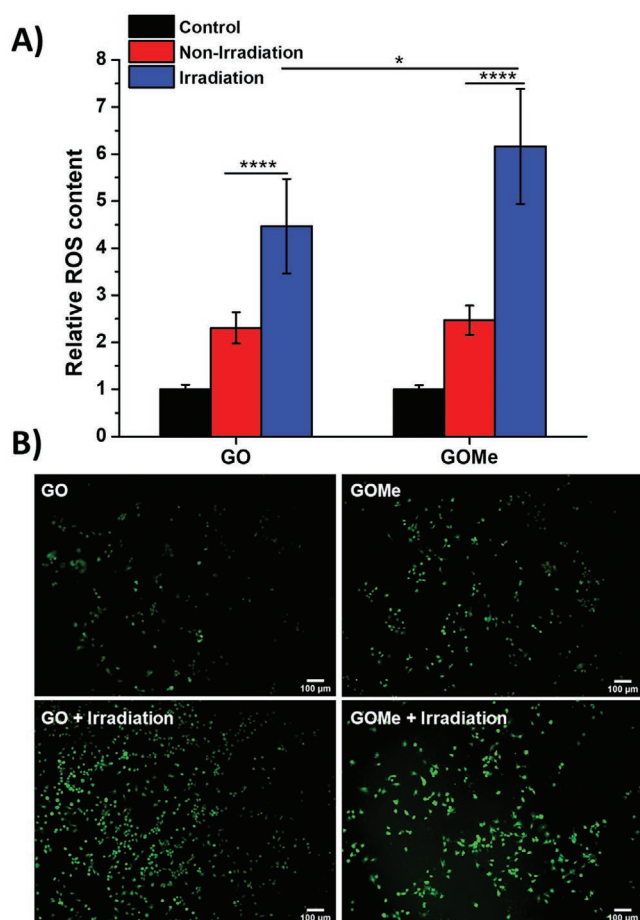


Figure 8. A) Relative ROS content after GO or GOMe treatment with or without irradiation. B) Fluorescence images of intracellular ROS with or without irradiation. MCF-7 cells were incubated with CM-H₂DCFDA reagent (excitation: 495 nm, emission: 527 nm) for 30 min before irradiation. The scale bar is 100 μm. The results are expressed as the means ± SD (*n* = 3). The statistical analyses were performed by the one-way ANOVA. **p* < 0.05; ***p* < 0.01; ****p* < 0.001; *****p* < 0.0001 compared to the untreated control.

of ROS, under NIR irradiation, resulting in potentially promising tools for a combined photodynamic and photothermal effect.^[49,50]

3. Conclusion

In summary, we have investigated the radical formation for the development of NIR phototherapy based on GO platform against breast cancer. We demonstrate that GO is a powerful PTT and PDT agent when excited in NIR region. Using a combination of fluorescent probes and spin traps, we shed the light on the radical photogeneration mechanism. When the sample is not irradiated, oxygenated radicals are generated, and this is associated with the electron transfer from GO to O₂. While during irradiation, there is a marked enhancement of ROS produced where ¹O₂ and O₂^{•−} are the radical species detected. Then, our study demonstrated how functionalization of GO through epoxide ring opening can tune the radical generation

affecting the ratio between superoxide and singlet oxygen produced. In particular, the introduction of reducing functions seems to reduce the ROS formation without irradiation and to favor the generation of O₂^{•−} during NIR irradiation. Then looking at the cellular effect of our previous observations, we pointed out the role of ROS-based PTT with GO conjugates in vitro and confirmed the trend observed in the mechanistic study. Based on the results we can conceive a new way to tune the properties of GO for a therapeutic use of PDT and PTT with only a single wavelength laser irradiation. Moreover, in the NIR range the tissues and the organs are transparent, limiting possible damages. All these results open the door to a better understanding of the interactions of the GO with light and within the cellular environment. With this work, we hope to inspire new studies unlocking the PDT potentials of GO and conceiving next generation “safe by design” materials and so linking drug delivery with heat and ROS generation. On the other hand, future studies using GO will need to focus on a systematic investigation of the presence of radicals before drawing any conclusions about the potential effects of GO. There are still many properties of GO to be explored, it is possible to imagine that the methods used to produce GO as well as the functionalization strategies can be designed to strengthen its phototherapeutic activity.

Supporting Information

Supporting Information is available from the Wiley Online Library or from the author.

Acknowledgements

The authors gratefully acknowledge the financial support from the EU Graphene Flagship project (881603) and from the Interdisciplinary Thematic Institute SysChem via the IdEx Unistra (ANR-10-IDEX-0002) within the program Investissement d’Avenir. This work was partly supported by the Centre National de la Recherche Scientifique (CNRS) through the International Research Project MULTIDIM between I2CT Unit and Okayama University, the International Center for Frontier Research in Chemistry (icFRC), and JST CREST (JPMJCR20H3). The French research infrastructure INFRANALYTICS FR2054 is acknowledged for its support. The authors thank B. Vileno for the helpful discussions. The authors are indebted to Cathy Royer from the Plateforme Imagerie In Vitro de l’ITI Neurostra for SEM analyses.

Conflict of Interest

The authors declare no conflict of interest.

Author Contributions

G.R. and A.B. conceived the idea and supervised the experiments. L.J., Z.S., and N.L.B. performed the experiments. All authors analyzed and discussed the data. A.B. acquired the funding. L.J. and Z.S. wrote the first draft. All authors edited and commented the final manuscript.

Data Availability Statement

The data that support the findings of this study are available from the corresponding author upon reasonable request.

Keywords

cancer phototherapies, carbon nanomaterials, chemical functionalization, photosensitizers, reactive oxygen species

Received: November 21, 2022

Revised: December 20, 2022

Published online:

- [1] C. Cha, S. R. Shin, N. Annabi, M. R. Dokmeci, A. Khademhosseini, *ACS Nano* **2013**, *7*, 2891.
- [2] H. Shi, P. J. Sadler, *Br. J. Cancer* **2020**, *123*, 871.
- [3] L. Zou, H. Wang, B. He, L. Zeng, T. Tan, H. Cao, X. He, Z. Zhang, S. Guo, Y. Li, *Theranostics* **2016**, *6*, 762.
- [4] Q. Cui, J.-Q. Wang, Y. G. Assaraf, L. Ren, P. Gupta, L. Wei, C. R. Ashby Jr., D.-H. Yang, Z.-S. Chen, *Drug Resistance Updates* **2018**, *41*, 1.
- [5] D. Kessel, *J. Clin. Med.* **2019**, *8*, 1581.
- [6] C. Backes, A. M. Abdelkader, C. Alonso, A. Andrieux-Ledier, R. Arenal, J. Azpeitia, N. Balakrishnan, L. Banszerus, J. Barjon, R. Bartali, S. Bellani, C. Berger, R. Berger, M. M. B. Ortega, C. Bernard, P. H. Beton, A. Beyer, A. Bianco, P. Bøggild, F. Bonaccorso, G. B. Barin, C. Botas, R. A. Bueno, D. Carriazo, A. Castellanos-Gomez, M. Christian, A. Ciesielski, T. Ciuk, M. T. Cole, J. Coleman, et al., *2D Mater.* **2020**, *7*, 022001.
- [7] D. De Melo-Diogo, R. Lima-Sousa, C. G. Alves, I. J. Correia, *Biomater. Sci.* **2019**, *7*, 3534.
- [8] D. de Melo-Diogo, R. Lima-Sousa, C. G. Alves, E. C. Costa, R. O. Louro, I. J. Correia, *Colloids Surf., B* **2018**, *171*, 260.
- [9] X. Sun, Z. Liu, K. Welscher, J. T. Robinson, A. Goodwin, S. Zaric, H. Dai, *Nano Res.* **2008**, *1*, 203.
- [10] S. Guo, S. Garaj, A. Bianco, C. Menard-Moyon, *Nat. Rev. Phys.* **2022**, *4*, 247.
- [11] C. Huang, X. Hu, Z. Hou, J. Ji, Z. Li, Y. Luan, *J. Colloid Interface Sci.* **2019**, *545*, 172.
- [12] A. B. Seabra, A. J. Paula, R. De Lima, O. L. Alves, N. Durán, *Chem. Res. Toxicol.* **2014**, *27*, 159.
- [13] L. Gonzalez, D. Lison, M. Kirsch-Volders, *Nanotoxicology* **2008**, *2*, 252.
- [14] L. Yang, R. Zhang, B. Liu, J. Wang, S. Wang, M. Y. Han, Z. Zhang, *Angew. Chem., Int. Ed.* **2014**, *53*, 10109.
- [15] C. Su, M. Acik, K. Takai, J. Lu, S. J. Hao, Y. Zheng, P. Wu, Q. Bao, T. Enoki, Y. J. Chabal, K. P. Loh, *Nat. Commun.* **2012**, *3*, 1298.
- [16] S. Vranic, A. F. Rodrigues, M. Buggio, L. Newman, M. R. H. White, D. G. Spiller, C. Bussy, K. Kostarelos, *ACS Nano* **2018**, *12*, 1373.
- [17] Y. Wang, F. Grote, Q. Cao, S. Eigler, *J. Phys. Chem. Lett.* **2021**, *12*, 10009.
- [18] Z. Komeily-Nia, L.-T. Qu, J.-L. Li, *Small Sci.* **2021**, *1*, 2000026.
- [19] F.-f. Zhao, S.-c. Wang, Z.-l. Zhu, S.-g. Wang, F.-f. Liu, G.-z. Liu, *Environ. Pollut.* **2019**, *249*, 1106.
- [20] M. Hada, K. Miyata, S. Ohmura, Y. Arashida, K. Ichiyonagi, I. Katayama, T. Suzuki, W. Chen, S. Mizote, T. Sawa, T. Yokoya, T. Seki, J. Matsuo, T. Tokunaga, C. Itoh, K. Tsuruta, R. Fukaya, S. Nozawa, S. I. Adachi, J. Takeda, K. Onda, S. Y. Koshihara, Y. Hayashi, Y. Nishina, *ACS Nano* **2019**, *13*, 10103.
- [21] J. Li, Q. Liu, D. Ho, S. Zhao, S. Wu, L. Ling, F. Han, X. Wu, G. Zhang, R. Sun, C. P. Wong, *ACS Appl. Mater. Interfaces* **2018**, *10*, 9727.
- [22] M. Gregoritz, F. P. Brandl, *Eur. J. Pharm. Biopharm.* **2015**, *97*, 438.
- [23] T. Soejima, K. Satoh, M. Kamigaito, *ACS Macro Lett.* **2015**, *4*, 745.
- [24] V. Froidevaux, M. Borne, E. Laborbe, R. Auvergne, A. Gandini, B. Boutevin, *RSC Adv.* **2015**, *5*, 37742.
- [25] N. Morimoto, T. Kubo, Y. Nishina, *Sci. Rep.* **2016**, *6*, 4.
- [26] Q. Mu, G. Su, L. Li, B. O. Gilbertson, L. H. Yu, Q. Zhang, Y. P. Sun, B. Yan, *ACS Appl. Mater. Interfaces* **2012**, *4*, 2259.
- [27] J.-W. Yoo, E. Chambers, S. Mitragotri, *Curr. Pharm. Des.* **2010**, *16*, 2298.
- [28] G. Reina, A. Ruiz, D. Murera, Y. Nishina, A. Bianco, *ACS Appl. Mater. Interfaces* **2019**, *11*, 7695.
- [29] B. Konkena, S. Vasudevan, *J. Phys. Chem. Lett.* **2012**, *3*, 867.
- [30] J. Ederer, P. Janoš, P. Ecorchard, J. Tolasz, V. Štengl, H. Beneš, M. Perchacz, O. Pop-Georgievski, *RSC Adv.* **2017**, *7*, 12464.
- [31] R. Li, N. D. Mansukhani, L. M. Guiney, Z. Ji, Y. Zhao, C. H. Chang, C. T. French, J. F. Miller, M. C. Hersam, A. E. Nel, T. Xia, *ACS Nano* **2016**, *10*, 10966.
- [32] M. Gutowski, S. Kowalczyk, *Acta Biochim. Pol.* **2013**, *60*, 1.
- [33] B. Ma, S. Guo, Y. Nishina, A. Bianco, *ACS Appl. Mater. Interfaces* **2021**, *13*, 3528.
- [34] R. Lauricella, B. Tuccio, in *Electron Paramagnetic Resonance Spectroscopy Applications* (Ed: P. Bertrand), Springer, Cham **2020**, Ch. 3.
- [35] F. A. Villamena, in *Reactive Species Detection in Biology: From Fluorescence to Electron Paramagnetic Resonance Spectroscopy* (Ed: F. A. Villamena), Elsevier, **2015**, Ch. 4.
- [36] M. Wrona, K. Patel, P. Wardman, *Free Radicals Biol. Med.* **2005**, *38*, 262.
- [37] G. Buettner, L. Oberley, *Biochem. Biophys. Res. Commun.* **1978**, *83*, 69.
- [38] T. Entradas, S. Waldron, M. Volk, *J. Photochem. Photobiol., B* **2020**, *204*, 111787.
- [39] L. M. Henderson, J. B. Chappell, *Eur. J. Biochem.* **1993**, *217*, 973.
- [40] C. Lee, J. S. Nam, C. G. Lee, M. Park, C. M. Yoo, H. W. Rhee, J. K. Seo, T. H. Kwon, *Nat. Commun.* **2021**, *12*, 26.
- [41] Y. He, A. Del Valle, Y. Qian, Y. F. Huang, *Nanoscale* **2017**, *9*, 1559.
- [42] Y. Nosaka, A. Y. Nosaka, *Chem. Rev.* **2017**, *117*, 11302.
- [43] S. Y. Qin, Y. J. Cheng, Q. Lei, A. Q. Zhang, X. Z. Zhang, *Biomaterials* **2018**, *171*, 178.
- [44] C. Martin, A. Ruiz, S. Keshavan, G. Reina, D. Murera, Y. Nishina, B. Fadeel, A. Bianco, *Adv. Funct. Mater.* **2019**, *29*, 1901761.
- [45] M. T. Vu, L. G. Bach, D. C. Nguyen, M. N. Ho, N. H. Nguyen, N. Q. Tran, D. H. Nguyen, C. K. Nguyen, T. T. H. Thi, *Int. J. Mol. Sci.* **2019**, *20*, 2016.
- [46] F. Viela, I. Navarro-Baena, A. Jacobo-Martín, J. J. Hernández, M. Boyano-Escalera, M. R. Osorio, I. Rodríguez, *RSC Adv.* **2018**, *8*, 22606.
- [47] D.-K. Ji, H. Dali, S. Guo, S. Malaganahally, J. Vollaie, V. Jossierand, H. Dumortier, C. Ménard-Moyon, A. Bianco, *Small Sci.* **2022**, *2*, 2100082.
- [48] B. Ma, Y. Nishina, A. Bianco, *Carbon* **2021**, *178*, 783.
- [49] X. Shi, H. Meng, Y. Sun, L. Qu, Y. Lin, Z. Li, D. Du, *Small* **2019**, *15*, 1901507.
- [50] D. K. Ji, G. Reina, S. Guo, M. Eredia, P. Samorì, C. Ménard-Moyon, A. Bianco, *Nanoscale Horiz.* **2020**, *5*, 1240.